INDIAN JOURNAL OF SCIENCE AND TECHNOLOGY

RESEARCH ARTICLE

Synthesis, Structural, Morphology and Magnetic Properties: Effect of La on Multiferroic Nature of $BiFeO_3$ Nanoparticles

Srinivas Perugu[1], G Bhanu Kiran[2], T Anil Babu[3], B V Raghavaiah[4]*

1 Department of Physics, Acharya Nagarjuna University, Guntur, 522510, India
2 Department of Mechanical Engineering, Rajiv Gandhi University of Knowledge Technologies (RGUKT), Nuzvid, 521201, India
3 Department of Physics, Andhra University, Visakhapatnam, 530003, India
4 Department of Physics, Rajiv Gandhi University of Knowledge Technologies (RGUKT), Ongole, 523001, India

OPEN ACCESS
Received: 28-08-2024
Accepted: 16-09-2024
Published: 10-10-2024

Citation: Perugu S, Bhanu Kiran G, Anil Babu T, Raghavaiah BV (2024) Synthesis, Structural, Morphology and Magnetic Properties: Effect of La on Multiferroic Nature of $BiFeO_3$ Nanoparticles. Indian Journal of Science and Technology 17(39): 4038-4047. https://doi.org/10.17485/IJST/v17i39.2761

* **Corresponding author**.
bv_raghavaiah@rediffmail.com

Funding: None

Competing Interests: None

Published By Indian Society for Education and Environment (iSee)

ISSN
Print: 0974-6846
Electronic: 0974-5645

Abstract

Objectives: The present study focuses on developing La-doped $BiFeO_3$ multiferroicmaterials for dielectric absorber applications. **Methods:** The samples are characterized by X-ray Diffractometer (XRD). Further, the morphology is examined using field emission electron microscopy (FESEM) and Transmission Electron Microscopy (TEM). The dielectric parameters and ac-electrical parameters are carried out by impedance spectroscopy. The magnetic properties are studied using a vibrating sample magnetometer VSM, P-E loop. **Findings:** XRD confirms the rhombohedral (trigonal) structure of BLFO nanoparticles. The grain and particle size values are determined by SEM and TEM, respectively. The dielectric and ac-electrical parameters for all the samples are thoroughly discussed at room temperature. The Maxwell-Wagner or interfacial polarization is noticed at low input field frequencies for x=0.2-0.8. The impedance analysis shows the contribution of grain and its boundary in the electrical conduction mechanism. The multiferroic behavior is examined using M-H loops, P-E loops, and μ_i-f plots. **Novelty:** The samples are synthesized by the hydrothermal process to prepare La-doped BiFeO3 nanomaterials.

Keywords: Nanoparticles; Electron Microscopy; Multiferroic; Magnetization; Polarization; Permeability

1 Introduction

Perovskite materials have been well-known to the scientific community for several years. Generally, among these perovskites, dielectric, ferroelectric, piezoelectric, pyroelectrics, ferromagnetic, and multiferroic materials achieved much more significance than other materials. As we know, the multiferroic perovskites show more than one ordering, such as magnetic, electric, elastic, etc. The magnetic ordering in multiferroics is established owing to the exchange interactions between magnetic dipoles within the ABO_3 perovskite structure. $BiFeO_3$ (BF) is a familiar multiferroic material that offers ferroelectricity, antiferromagnetism, and ferroelasticity. As a result, bismuth iron oxide attracted the scientific community to work further on it to study various optical, mechanical, photocatalytic, and electrical properties. Moreover, the BF exhibits a rhombohedral distorted structure and offers applications in memory, spintronic, photocatalytic, and photovoltaic devices[1]. However, BF has difficulties providing low retentivity, weak magnetization, low polarization, and high leakage current[1]. To avoid this problem, the rare earth elements must be incorporated into the BF perovskite system. Thus, it may enhance the magnetization and polarization behavior, decreasing leakage current.

1.1 Related work

Based on previuos reports, BF, and La doped BF materials were synthesized through different methods and prepared nano partcicles size ranges in between 50 -150 nm, and studied the effect of synthesis method on different properties like structure, electrical, dilectric and magnetic. Like the two-step anodization process[2], solid-state reaction technique, sol-gel method[3–6], ball-milled method[7,8], and spark plasma sintering[9]. Using different synthesis methods, it is observed that the structural, electrical, optical, and magnetic properties have been optimized.

1.2 Research Gap

The literature survey indicates that the La-doped BiFeO3 nanoparticles are synthesized via different synthesis methods like Sol-Gel, auto combustion, solvothermal, hydrothermal, Pechini methods, etc.[1–17]. All the reports evidenced that the complete study on structure, morphology, dielectric, magnetic, ferroelectric, and impedance behavior is not provided in the literature.

1.3 Contributions

In the present study, our contributions are as follows:

1. We have prepared the La-doped $BiFeO_3$ nanomaterials by Hydrothermal method at low reaction temperature as it possesses a few significant benefits like easy preparation, less time-consuming, low operating temperatures, inexpensive, good crystallinity, high homogeneity, etc.
2. Further, the materials are characterized by XRD, FESEM, TEM, Impedance spectroscopy, VSM, and PE loops.

2 Methodology

The hydrothermal synthesis is employed to prepare $Bi_{1-X}La_XFeO_3$ (X = 0.2-0.8) (BLFO) nanoparticles (Figure 2). The starting materials are $La(NO_3)_3.6H_2O$ (99.8 % purity, Sigma-Aldrich), $Bi(NO_3)_3{\cdot}5H_2O$ (99.8 % purity, Sigma-Aldrich), and $Fe(NO_3)_3{\cdot}9H_2O$ (99.9 % purity, Sigma-Aldrich). The details of the preparation method can be seen in[18]. The characterization is carried out by XRD, TEM, SEM, Vibrating sample magnetometer VSM, P-E loop (Marain India Ltd.), and LCR controller (HIOKI 3532-50, 42 Hz–5 MHz) to study the structural, morphological, magnetic, ferroelectric, and dielectric properties, respectively.

3 Results and Discussion

The X-ray diffraction spectra of BLFO nanoparticles are shown in Figure 1. It was found from the XRD patterns that the x=0.2-0.8 samples showed well crystalline peaks. The single-phase structure was attributed to all samples, including a few secondary phases. These secondary phases were incurred owing to the orthorhombic $Bi_2Fe_4O_9$ and cubic $Bi_{25}FeO_{40}$. The single phases were compared with standard JCPDS: 86-1518. The maximum intensity was recorded at (110) plane. It was also observed that the secondary phases almost disappeared owing to the increase of La-content above 50 % in the BLFO system. This established that the high La-content induced the reduction of secondary phases. Besides, the average crystallite size (D_{avg}) was calculated using the Scherrer equation: $D=0.9\lambda/\beta Cos\theta$, where '$\beta$' is the full-width half maxima, and 'θ' is the angle of diffraction[17]. The results are listed in Table 1. It was understood from these results that the D_{avg} values were increased from 41.5 to 83.6 nm as a function of composition from x=0.2-0.8. This can be ascribed to the decreased full-width half maxima (FWHM) or microstrain from 0.0034 to 0.0012 with an increase in the 'x' value. Further, the lattice constants were calculated and mentioned in Table 1. The values were increased from 0.5599-0.5619 nm (a=b) and 1.3926-1.3952 nm with an increase in 'x'. This trend was attributed to the effect of ionic radii difference between the dopant and parent element. As per the Shannon ionic radii table[17], the ionic radii of elements were noted to be La^{+3}: 0.136 nm, Bi^{+3}: 0.096 nm, and Fe^{+3}: 0.0645 nm. These values showed that the La^{+3} cations cannot replace the Fe^{+3} cations as the site will fluctuate due to its loose position. Hence, the La^{+3} ions can easily replace the Bi^{+3} cations. The ionic radii of La^{+3} cations are higher than those of the ionic radii of the ionic radii of Bi^{+3} cations. Therefore, the unit cell dimensions will be increased upon the replacement of Bi^{+3} ions by La^{+3} ions. In this connection, the unit cell volume V_{cell} was increased from 0.4365 to 0.4405 nm^3 with 'x'. Further, the c/a ratio was almost constant, varying in the third decimal from 2.487 to 2.483. The X-ray density (ρ_x=Z*M.W./(N*V) (for trigonal Z = 1, where Z = effective number of atoms per unit cell, M.W is the molecular weight of the composition, N is the Avogadro's number ($6.023x10^{23}$). V is the unit cell volume) was decreased from 1.136 to 0.968 g/c.c., as a function of 'x'. This trend was ascertained by the decrease in molecular weight (MW) from 298.81 to 256.76 g/mol. Besides, the low densities were obtained due to the porous structure followed by high dislocation density. Moreover, synthesized samples (not sintered at high temperatures) can usually show small density values. Later, the specific surface area was calculated using a formula S=600/D_{avg}*ρ_x, where the symbols have their usual meaning. The results indicated that the 'S' values decreased from 127.2 to 74.2 m^2/g with 'x'. This evidenced that the 'S' values were inversely proportional to the 'D_{avg}' values. A similar type of observation was seen in the literature[16,17]. The surface morphology was examined using the FESEM and HRTEM. The FESEM images are shown in Figure 2. It was observed from these images that the evolution of nanorods was eventually increasing from x=0.2-0.8. That means the increase of La-content in the BFO system induces the formation of nanorod-like morphology. However, few nanospheres like grains were seen among these nanorods. The nucleation process can be responsible for this kind of behavior. Due to the high difference in ionic radii of the cations, the site will start fluctuating in different directions. Hence, the nanospheres' deformation in horizontal or vertical directions. Therefore, the distortions will be formed, leading to the formation of nanorods-like structures in the morphology. Thus, in the case of x=0.2-0.8, the nanorod-like morphology appeared.

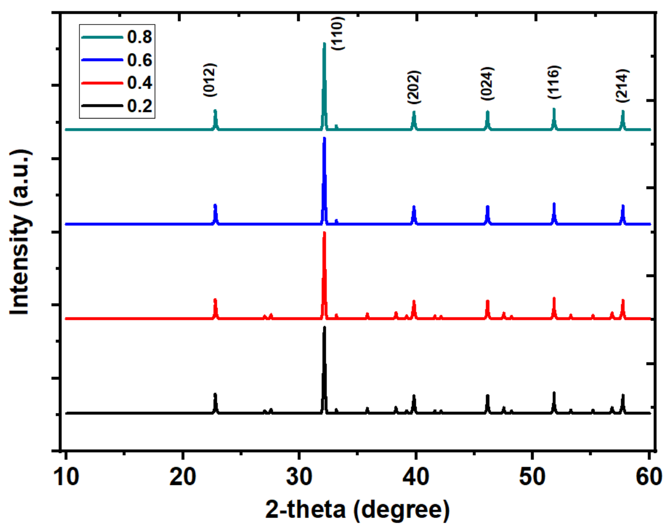

Fig 1. XRD patterns of BLFO nanoparticles

Table 1. Structural parameters of BLFO nanoparticles

X	**0.2**	**0.4**	**0.6**	**0.8**
D_{avg} (nm)	41.5	60.2	68.6	83.6
FWHM β_{avg} (^{o})	0.0034	0.0024	0.0019	0.0012
a = b (nm)	5.599	5.604	5.612	5.619
c (nm)	13.926	13.932	13.944	13.952
c/a ratio	2.487	2.486	2.485	2.483
MW (g/mol)	298.81	284.79	270.78	256.76
V_{cell} $(nm)^3$	0.4365	0.4375	0.4392	0.4405
ρ_x (g/cm^3)	1.136	1.081	1.024	0.968
P_{avg} (nm)	74.8	92.4	116.1	127.4
S (m^2/g)	127.2	92.2	85.4	74.2

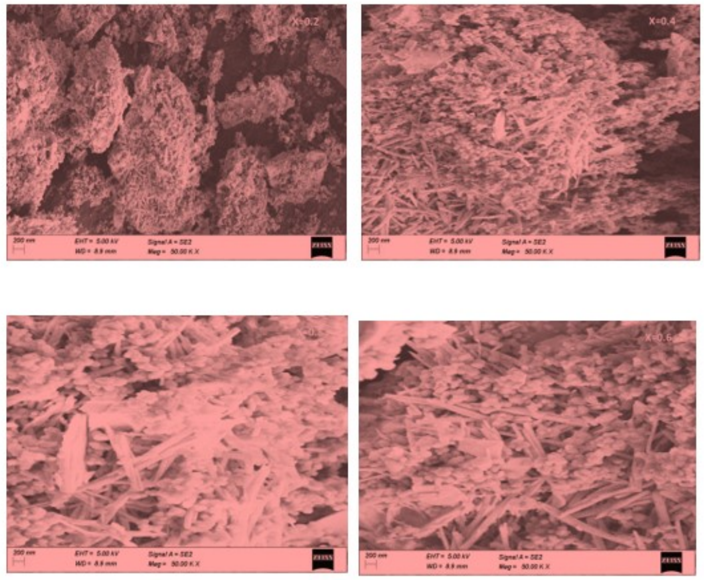

Fig 2. FESEM images of BLFO nanoparticles

The average grain size was determined using the linear intercept method, wherein the formula Gavg=1.5L/MN (where L indicates the test line length, M indicates the magnification, and N indicates the number of grains intersecting the test line) was used[18,19]. The results ensured that the grain size increased from 96.4 to 168.3 nm with 'x'. This was attributed to the decrease of internal microstrain reported in the literature[20]. Further, the HRTEM images (Figure 3) also showed the nanorods-like particles, including the nanospheres. The particle size was found to vary from 74.8 to 127.4 nm as a function of 'x'. Overall, it was understood that the variation trend of crystallite size, grain size, and particle size values followed a similar order with an increase in La-content in the BFO system.

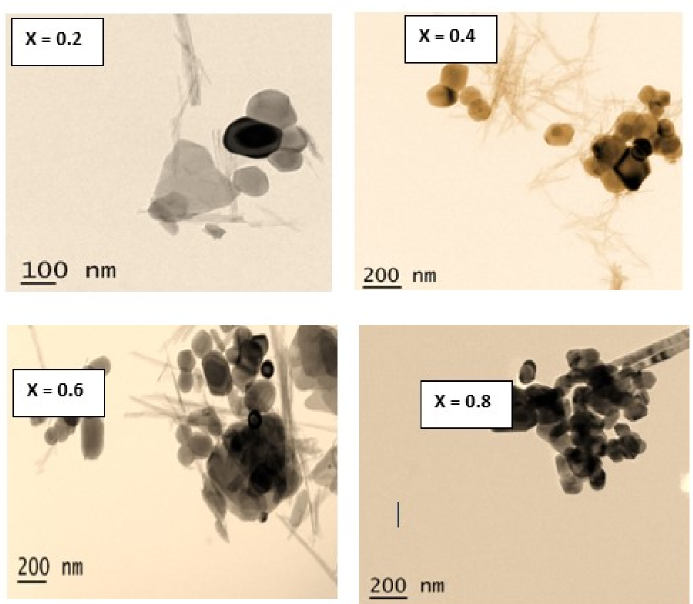

Fig 3. TEM images of BLFO nanoparticles

The room temperature dielectric properties were studied using an LCR controller as a function of composition (from x=0.2-0.8) and frequency (from 42 Hz-5 MHz). The dielectric parameters viz., real part of permittivity (ε') and imaginary part of permittivity (ε") were carried out for all samples. Herein, the real part indicates the dielectric constant (energy stored), and the imaginary part shows the dielectric loss (energy dissipated)[19]. The frequency-dependent dielectric constant and dielectric loss plots are shown in Figure 4**a** and **b** respectively. It was understood from the dielectric constant versus frequency plots that the dielectric constant was noted to be very high at low frequencies. Eventually, the dielectric constant was decreased to small values till log ω = 5.864. Beyond log ω = 5.864, the resonance behavior was noticed. The reasons behind these observations are as follows: The high magnitude values of dielectric constant were attributed to the space charge polarization mechanism. That is, the grain boundaries could be responsible for this. At the small frequencies, the charges will be piled up at the grain boundaries (high resistive layers). Hence, the carriers will be stopped at these layers. For further frequency increase, the carriers can attain higher energy than the grain boundary energy. As a result, the grain boundary will be broken up, so the polarization mechanism comes down. Therefore, one can get a high dielectric constant at low frequencies while the same parameter will be less at high frequencies. The frequency match of the electric field and oscillating dipole can lead to the resonance or relaxation trend that is shown in Figure 4 **c**. Similarly, the dielectric loss plots (Figure 4) showed the high dielectric loss at low frequencies, whereas the low loss values were obtained at high frequencies. This is attributed to the grain effect. Besides, the relaxations were seen at two frequencies, such as log ω=5.483 & 7.492. The simplified data of dielectric parameters was listed in Table 2 at a few selected frequencies like 100 Hz, 10 kHz, 100 kHz, 1 MHz, and 5 MHz.

Table 2. Data on dielectric parameters of BLFO nanoparticles

x	0.2	0.4	0.6	0.8
		ε'		
100 Hz	41.5	82.9	346.2	174.8
10 kHz	17.5	33.4	35.1	79.3
100 kHz	10.3	19.4	16.4	45.1
1 MHz	10.9	21.4	17.8	37.9
5 MHz	2.1	4.5	3.9	6.4
		ε"		
100 Hz	93.9	166.9	116.1	290.2
10 kHz	17.0	13.2	29.3	25.3
100 kHz	4.8	5.1	10.6	15.4
1 MHz	1.9	5.3	5.5	11.5
5 MHz	2.0	6.8	5.9	15.5
		Log σ_{ac} (S/cm)		
100 Hz	-8.282	-8.0324	-8.189	-7.792
10 kHz	-7.805	-7.736	-7.469	-7.308
100 kHz	-6.953	-6.540	-6.507	-6.243
1 MHz	-5.996	-5.689	-5.749	-5.252
5 MHz	-5.072	-4.636	-4.727	-4.310
		Log σ_{dc} (S/cm)		
	-6.869	-6.612	-6.536	-6.186

The values showed that the dielectric constant and loss parameters were increasing with an increase in 'x'. The high dielectric constant dielectric loss values were seen for the x=0.8 sample. Hence, this sample may be suitable for dielectric absorber applications. Later, the frequency dependence of electrical conductivity (σ_{ac}= $\varepsilon_o\varepsilon$") was depicted in Figure 4**c** (log σ_{ac} versus log ω). Using the power law equation: σ_{ac} = Aω^n+ σ_{dc} (σ_{ac} (f, T) + σ_{ac} (T)), the dc-electrical conductivity values were determined by extrapolating the straight line towards the Y-axis[20].

The intersecting portion indicates the σ_{dc}. The σ_{ac} & σ_{dc} values are listed in Table 2. The σ_{ac} values were increasing with frequency for x=0.2-0.8. This was incurred due to the hopping of electrons between ferric and ferrous ions. Both the conductivity values increased with the increase of La-content. This kind of trend was generally attributed to the hopping conduction mechanism at room temperature. Moreover, the exponent (n) values were evaluated and found to be varying from 0.364 to 0.872.

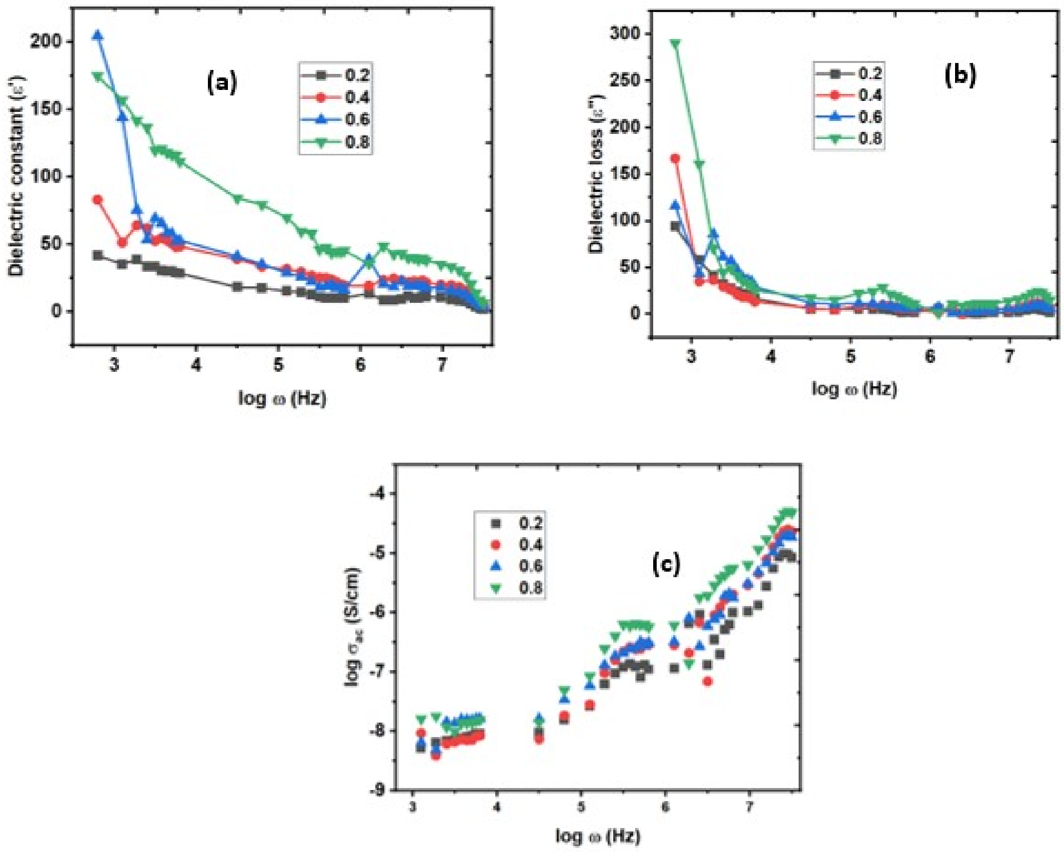

Fig 4. (a) Dielectric constant versus frequency plots of BLFO nanoparticles (b) Dielectric loss versus frequency plots of BLFO nanoparticles, and (c) AC-conductivity versus frequency plots of BLFO nanoparticles

This evidenced the fact that the M_r/M_s values were less than 0.5. The multi-domain magnetic nanoparticles will indicate the squareness values less than half. That means the present BLFO nanoparticles can be multi-domain magnetic[21]. The coercivity (H_c) was found to vary from 439.3-758.4 Oe., as a function of 'x' Figure 5**a, b**. The variation trend was noticed to be unsystematic, and the grain size effect, domain wall displacement, domain wall rotation, and dopant may have caused it. Later, the anisotropy constant $K_1 = H_c M_s/0.96$ and magnetic moment nB = M.W.*Ms/5585[21] were calculated and listed in Table 3. The results ensured that the K1 varied from 6845-12640 erg/c.c., with 'x' unsystematically. Likewise, the magnetic moment decreased from 3.41-2.55 μB/f.u., with an increase in 'x'. This behavior was attributed to decreased compositional molecular weight, as listed in Table 1. Although the magnetization increased, the magnetic moment decreased with composition. This happened due to the magnetic moment's strong dependence on the composition's molecular weight. Besides, the initial permeability (μ_i) versus log ω plots were drawn, as shown in Figure 6.

Table 3. Magnetic parameters of BLFO nanoparticles

x	0.2	0.4	0.6	0.8
M_s (emu/g)	13.2	16.0	17.1	21.5
M_r (emu/g)	6.0	7.9	4.8	5.6
M_r/M_s	0.455	0.494	0.281	0.261
H_c (Oe.)	497.8	758.4	439.3	449.1
K_1 (erg/c.c)	6845	12640	7825	10058
n_B (μB/f.u.)	3.41	2.74	2.64	2.55

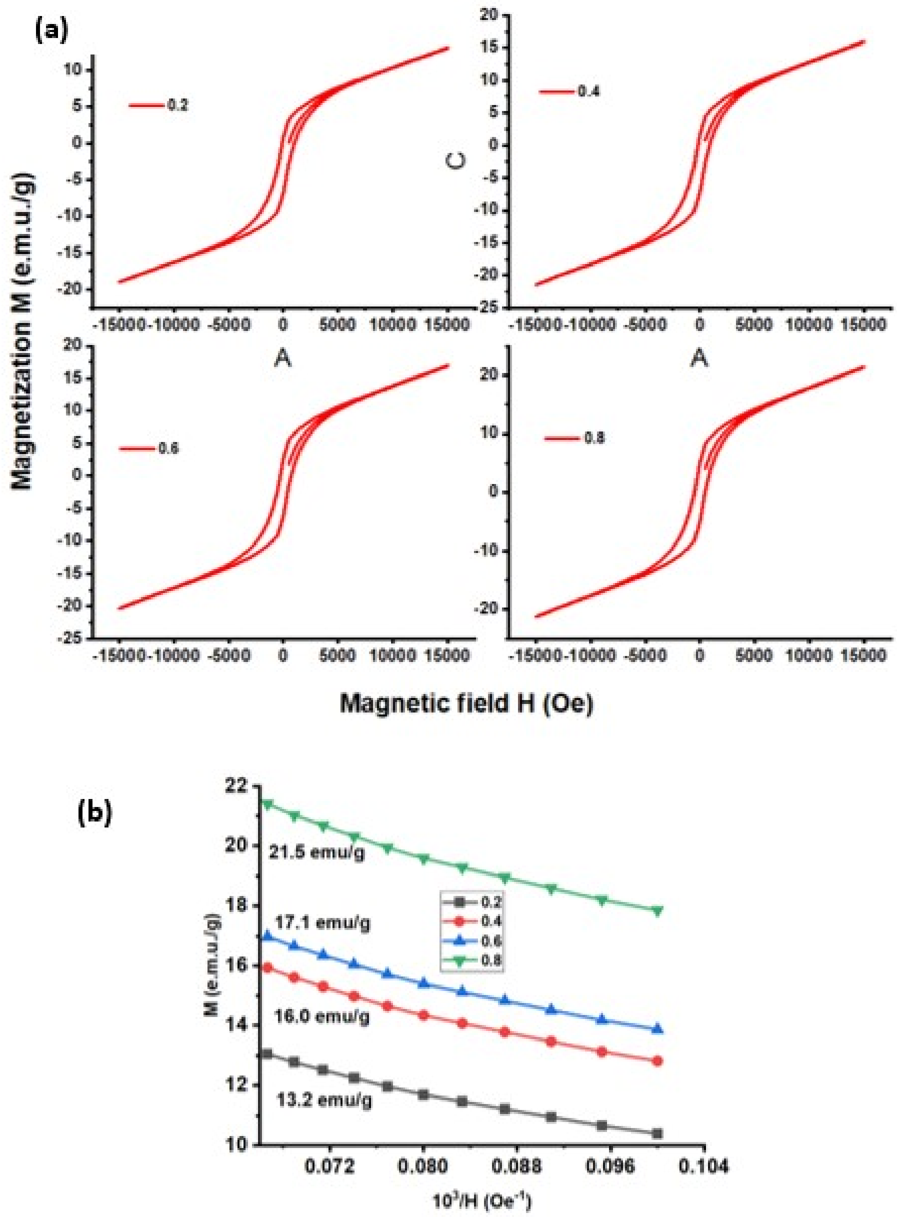

Fig 5. (a) M-H loops of BLFO nanoparticles, (b) LAS plots of BLFO nanoparticles

The μ_i values of x=0.2-0.8 samples were very small at low magnetic field frequency. For further frequency increase, the μi values gradually increased and suddenly reached the maximum value at log ω = 4.1 & 5.68 for x=0.2-0.8. Two relaxation peaks were seen in the BLFO samples. This occurred due to the multiferroic nature. The first relaxation peak was formed due to its ferroelectric nature, while the other one was produced due to its ferromagnetic nature. At these relaxations, the x=0.2-0.8 samples offered high permeability. This kind of trend was generally formed owing to the matching of input field frequency with the oscillating electric/magnetic dipoles[22]. The compositional dependence of permeability confirmed that the μ_i was decreasing from 5.24 to 4.14 for x=0.2-0.6 (at 5 MHz). For x=0.8, it was found to be increasing to 4.96 (at 5 MHz). This kind of behavior was achieved due to the presence of variable exchange interaction among ferric and ferrous ions. Further, the ferroelectric hysteresis nature of x=0.2-0.8 was analysed using the P-E loops (Figure 7). It was observed from the P-E loops that the 'banana' shape was predominant for x=0.2-0.8. This indicated fact that the oxygen vacancies seemed to be high in

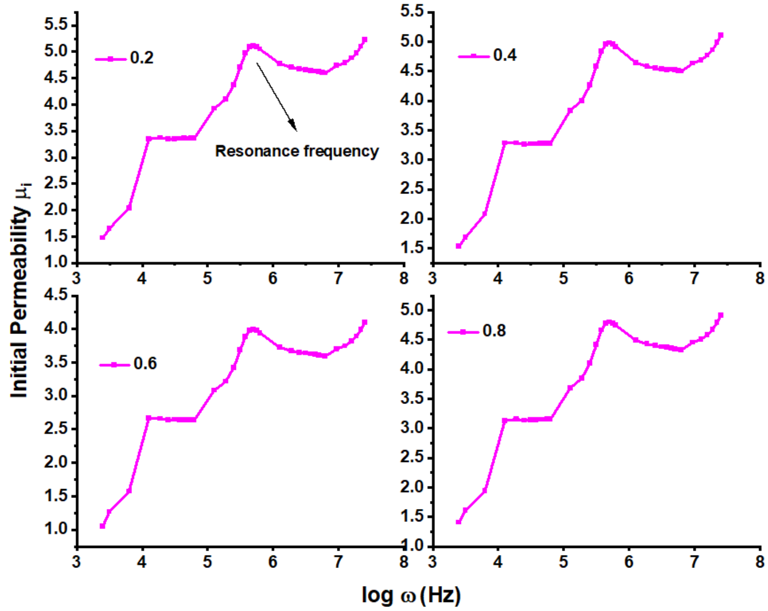

Fig 6. Initial permeability (μ_i) versus log ω plots of BLFO nanoparticles

concentration. Due to this, the 180° ferroelectric spins will be predominant. A similar nature was discussed earlier by several scientists[23,24]. Moreover, this showed the weak ferroelectric nature wherein the bismuth cations could be responsible for this nature. The coercive electric field was noticed to be altering from 0.2-0.56 kV/cm as a function of 'x'. The remanence polarization seemed to change from 0.0024-0.0048 μC/cm2 with an increase in 'x'. Moreover, the variation trend was unsystematic with composition[17].

The present study results are well compared with the reported in the literature[5,7,24].

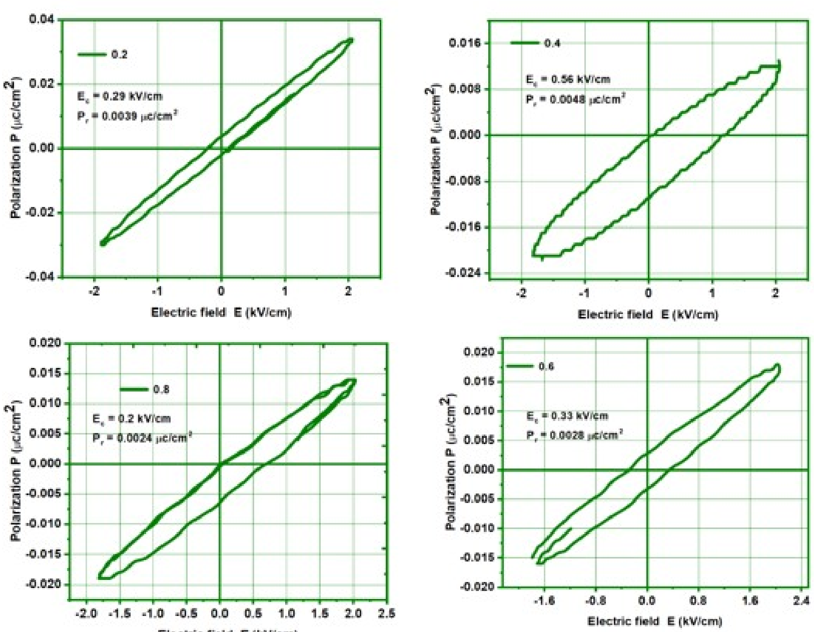

Fig 7. P-E loops of BLFO nanoparticles

4 Conclusion

The $Bi_{1-X}La_XFeO_3$ (X = 0.2-0.8) nanoparticles were successfully prepared using hydrothermal methods. The XRD patterns confirmed the rhombohedral phase structure, including some secondary peaks. Herein, the high La-content reduced the number of secondary phases. Further, the morphology (FESEM & HRTEM) suggested the formation of nanorods-like structures. The space charge polarization was well observed among the dielectric properties. La dopant optimized the conductivity properties of BFO samples. The saturation magnetization (M_s) values were increased from 13.2 to 21.5 emu/g as a function of 'x' from 0.2-0.8. Later, the squareness (M_r/M_s) values were computed and found to be altering from 0.261-0.494, which evidenced the existence of a multi-domain magnetic nature. The linear and unsaturated loops suggest the antiferromagnetic nature of ceramics. Two relaxations were seen in the permeability versus frequency plots, suggesting the multiferroic nature of BLFO samples. The P-E loops of x=0.2-0.8 showed the 'banana' shape, indicating the presence of oxygen vacancies. The sample $Bi_{1-X}La_XFeO_3$ (X = 0.8) showed high dielectric constant dielectric loss values. Therefore, these materials are suggested for dielectric absorber applications.

References

1) Delfard NB, Maleki H, Badizi AM, Taraz M. Enhanced Structural, Optical, and Multiferroic Properties of Rod-Like Bismuth Iron Oxide Nanoceramics by Dopant Lanthanum. *Journal of Superconductivity and Novel Magnetism*. 2020;33:1207–1214. Available from: https://doi.org/10.1007/s10948-019-05294-3.
2) A-Ur-Rehman, Ashraf MW, Tayyaba S, Ali SM, Ramay SM, Saleem M. BiFeO3 and La doped BiFeO3 nano-particles decorated anodic Al2O3 porous template fabricated with two step anodization. *Materials Letters*. 2019;244(1):115–118. Available from: https://doi.org/10.1016/j.matlet.2019.02.061.
3) Kumar P, Chand P, Singh V. La3+ substituted BiFeO3-a proficient nano ferrite photo-catalyst under the application of visible light. *Chemical Physics Letters*. 2020;754:137715–137715. Available from: https://doi.org/10.1016/j.cplett.2020.137715.
4) Kumar KS, Ramu S, Sudharani A, Ramanadha M, Murali G, Vijayalakshmi RP. Enhanced magnetic and dielectric properties of Gd doped BiFeO3: Er nanoparticles synthesized by sol-gel technique. . *Physica E: Low-dimensional Systems and Nanostructures*. 2020;734:137715. Available from: https://doi.org/10.1016/j.physe.2019.113689.
5) Lans YC, Sun F, Chen Y, Chen D, Mai W, Zhu M. Tuning piezoelectric driven photocatalysis by La-doped magnetic BiFeO3-based multiferroics for water purification. *Nano Energy*. 2022;93:106792–106792. Available from: https://doi.org/10.1016/j.nanoen.2021.106792.
6) Amin M, Rafique HM, Mustafa GM, Mahmood A, Ramay SM, Atiq S, et al. Effect of La/Cr co-doping on dielectric dispersion of phase pure BiFeO3 nanoparticles for high frequency applications. *Journal of Materials Research and Technology*. 2021;13:1534–1545. Available from: https://doi.org/10.1016/j.jmrt.2021.05.066.
7) Pedro-García F, Betancourt-Cantera LG, Bolarín-Miró AM, Cortés-Escobedo CA, Barba-Pingarrón A, Jesús FSD. Magnetoelectric coupling in multiferroic BiFeO3 by co-doping with strontium and nickel. *Ceramics International*. 2019;45(8):10114–10119. Available from: https://doi.org/10.1016/j.ceramint.2019.02.058.
8) Kumar S, Srivastava G, Almutairi G, Ahmed F, Shaalan NM, Dalela S, et al. Electronic structure and electrochemical properties of La-doped BiFeO3 nanoparticles. *Journal of Electron Spectroscopy and Related Phenomena*. 2021;253:147138–147138. Available from: https://doi.org/10.1016/j.elspec.2021.147138.
9) Oliveira RC, Volnistem EA, Astrath E, Dias GS, Santos IA, Garcia D, et al. La doped BiFeO3 ceramics synthesized under extreme conditions: Enhanced magnetic and dielectric properties. *Ceramics International*. 2021;47(14):20407–20412. Available from: https://doi.org/10.1016/j.ceramint.2021.04.049.
10) Anburaja R, Shaik K. Synthesis and Characterizations of BiFeO3 Nanoparticles for Photocatalytic Application. *Chemistry Select*. 2024;9:202402257–202402257. Available from: https://doi.org/10.1002/slct.202402257.
11) Amdouni W, Fricaudet M, Otoničar M, Garcia V, Fusil S, Kreisel J, et al. BiFeO3 Nanoparticles: The "Holy-Grail" of Piezo-Photocatalysts? *Advanced Materials*. 2023;35:2301841–2301841. Available from: https://doi.org/10.1002/adma.202301841.
12) Parida S, Nanda J, Sarangi B. Investigation of structural, optical, magnetic and photocatalytic properties of Eu-Mg co-doped BiFeO3 nanoparticles. *Journal of Sol-gel Science and Technology*. 2024;109:150–161. Available from: https://doi.org/10.1007/s10971-023-06257-.
13) Carranza-Celis D, Cardona-Rodríguez A, Narváez J. Control of Multiferroic properties in BiFeO3 nanoparticles. *Scientific Reports*. 2019;9:3182–3182. Available from: https://doi.org/10.1038/s41598-019-39517-3.
14) Papadopoulos K, Myrovali E, Malletzidou L, Karfaridis D. Control of multiferroic features in BiFeO3 nanoparticles by facile synthetic parameters. *Ceramics International*. 2023;49(11B):18552–18564. Available from: https://doi.org/10.1016/j.ceramint.2023.02.229.
15) Wrzesińska A, Khort A, Witkowski M. Structural, electrical, and magnetic study of La-, Eu-, and Er- doped bismuth ferrite nanomaterials obtained by solution combustion synthesis. *Scientific Reports*. 2021;11:22746–22746. Available from: https://doi.org/10.1038/s41598-021-01983-.
16) Zhang L, Li X, Chen J, Jin D, Cheng J. Enhanced photocatalytic activity in ferroelectric BiFeO3 nanoparticles treated by a corona poling method. *Ceramics International*. 2022;48(11):15908–1591. Available from: https://doi.org/10.1016/j.ceramint.2022.02.131.
17) Balmuchu SP, Dobbidi P. The effect of La doping on multiferroic BiFeO3 ceramic through structural, dielectric, magnetic, ferroelectric, and optical studies. *In Physica B: Condensed Matter Physics*. 2022;638:413937–413937. Available from: https://doi.org/10.1016/j.physb.2022.413937.
18) Raghuram N, Rao TS, Naidu KC. Magnetic properties of hydrothermally synthesized Ba1-xSrxFe12O19 (x = 0.0-0.8) nanomaterials. *Applied Physics*. 2019;125:839–839. Available from: https://doi.org/10.1007/s00339-019-3143-2.
19) Kumar DS, Naidu K, Rafi MM, Nazeer KP, Begam AA, Kumar GR. Structural and dielectric properties of superparamagnetic iron oxide nanoparticles (SPIONs) stabilized by sugar solutions. *Materials Science-Poland*. 2018;36(1):123–133. Available from: https://doi.org/10.1515/msp-2018-0017.
20) Sagar TV, Rao ST, Naidu KCB. Effect of calcination temperature on optical, magnetic and dielectric properties of Sol-Gel synthesized Ni0. *Ceramics International*. 2020;46:11515–11529. Available from: https://doi.org/10.1016/j.ceramint.2020.01.178.
21) Naidu KCB, Madhuri W. Effect of non-magnetic Zn2+ cations on initial permeability of microwave treated NiMg ferrites. *International Journal of Applied Ceramic Technology*. 2016;13:1090–1095. Available from: https://doi.org/10.1111/ijac.12571.
22) Kumar NS, Suvarna RP, Naidu KCB. Structural and ferroelectric properties of microwave heated lead cobalt titanate nanoparticles synthesized by sol–gel technique. *Journal of Materials Science: Materials in Electronics*. 2018;29(6):4738–4742. Available from: https://dx.doi.org/10.1007/s10854-017-8429-6.

23) Raghuram N, Rao TS, Naidu KCB. Electrical and impedance spectroscopy properties of hydrothermally synthesized Ba0.2Sr0.8-yLayFe12O19 (y = 0.2–0.8) nanorods. *Ceramics International*. 2020;46(5):5894–5906. Available from: https://dx.doi.org/10.1016/j.ceramint.2019.11.042.
24) Dastagiri S, Lakshmaiah MV, Naidu KCB, Kumar NS, Khan A. Induced dielectric behavior in high dense AlxLa1-xTiO3 (x=0.2–0.8) nanospheres. *Journal of Materials Science: Materials in Electronics*. 2019;30(22):20253–20264. Available from: https://dx.doi.org/10.1007/s10854-019-02409-3.